in silico plants, 2024, **6**, 1–13
https://doi.org/10.1093/insilicoplants/diae001
Advance Access Publication 14 February 2024
Original Article

Original Article

A mathematical model of photoinhibition: exploring the impact of quenching processes

Tim Nies[1], Shizue Matsubara[2,3], and Oliver Ebenhöh[1,3,*]

[1]Institute of Quantitative and Theoretical Biology, Heinrich Heine University Düsseldorf, Universitätsstraße 1, 40225 Düsseldorf, Germany
[2]IBG-2: Plant Sciences, Forschungszentrum Jülich, 52425 Jülich, Germany
[3]Cluster of Excellence on Plant Sciences (CEPLAS), Universitätsstraße 1, 40225 Düsseldorf, Germany

*Corresponding author's e-mail address: oliver.ebenhoeh@hhu.de

Handling editor: Xin-Guang Zhu

ABSTRACT

Plants are constantly exposed to changing environments, sometimes leading to extreme conditions and stress. For example, sudden exposure to high light leads to excess absorbed light energy, causing reactive oxygen species (ROS) formation. ROS damages the photosynthetic machinery, particularly the D1 protein in photosystem II (PSII), which, therefore, needs to be continuously repaired and replaced. The effect of the damage inflicted by high light is a prolonged decrease in photosynthetic efficiency. Hence, it is not surprising that photoinhibition has been subject to numerous experimental studies investigating its effects in the context of crop productivity. However, it has become apparent that classical measures of photoinhibition, that is, changes in the chlorophyll fluorescence parameter F_v/F_m, are not only determined by the loss of PSII core function but also by processes such as energy transfer and quenching. Mathematical models can help dissect the influences on such fluorescence signals and quantify the contributions of various interacting mechanisms. We present a mathematical model with a dynamic description of the photosynthetic electron transport chain, non-photochemical quenching and photoinhibition. With our model, we investigate the interconnection among quenching, photoprotection and fluorescence using simulations and experimental data. We found that different energy-dissipating properties of intact and damaged PSIIs, as well as energy transfer between PSIIs, are critical components that need to be included in the model to ensure a satisfactory fit to the experimental data. We envisage that our model provides a framework for future investigations of photoinhibition dynamics and its importance for plant growth and yield.

KEYWORDS: Fluorescence; high light stress; mathematical model; photoinhibition; quenching.

1. INTRODUCTION

Photosynthesis is one of the main processes that make energy available to the biosphere (Ksenzhek and Volkov, 1998). By capturing light, photosynthetic organisms convert solar energy into usable chemical energy, which is then used to drive metabolic processes, including the formation of biomass. Plants, algae and other photosynthetic organisms exist in a wide range of environments, ranging from deserts to tropical forests. These environments can exhibit drastically and rapidly changing external conditions, considering, for example, light intensity, temperature and humidity. Plants, as sessile organisms, must adapt to the conditions they are exposed to (Kaiser *et al.*, 2018). However, such fluctuating conditions make the coordination of the photosynthetic electron transport chain (PETC), supplying light energy in the form of adenosine triphosphate (ATP) and NADPH, and the Calvin Benson Bassham cycle (CBB cycle), which uses ATP and NADPH to sequester CO_2, a challenging task (Nies *et al.*, 2023). Antenna complexes in chloroplast thylakoid membranes collect light energy and channel it to the reaction centers of the PETC. This captured energy is used to drive photochemistry, but the excited states can also dissipate energy as heat or re-emit it as fluorescence (Muller *et al.*, 2001). Due to variations in external conditions, the light energy supply can frequently exceed the demand, which leads to the formation of reactive oxygen species (ROS) at multiple sites of the PETC. ROS are highly reactive compounds that can damage the molecular machinery of the PETC (Khorobrykh *et al.*, 2020).

The photodamage induced by ROS affects various proteins, with the D1 subunit of photosystem II (PSII) being the most susceptible. In fact, with a turnover rate of $> 0.5\ d^{-1}$, the D1 subunit exhibits one of the shortest protein lifetimes in the

PETC (Li *et al.*, 2018). For functional photosynthesis, it is, therefore, essential that this protein is constantly resynthesized and replaced. This is realized by the so-called D1 protein repair cycle, which involves the degradation and synthesis of damaged D1 protein. This cycle has a very high energy demand, with an estimated 1304 ATP per subunit repaired (Murata and Nishiyama, 2018). Despite considerable advances in our understanding of photoinhibition, the exact mechanism of how high-light stress inflicts damage on the photosynthetic machinery is still under debate, and various hypotheses have been proposed (Zavafer, 2021).

Classically, photoinhibition is quantified by measuring F_v/F_m after prolonged exposure to strong irradiance. This was justified because of the almost linear relationship between F_v/F_m and the loss of photosynthetic O_2 evolution (see, e.g. Patsikka *et al.*, 1998). It has recently become increasingly apparent that the F_v/F_m, derived from the fluorescence signal, might not be ideal for assessing photoinhibition. The fluorescence signal that a photosynthetic tissue, such as a leaf, emits is influenced by multiple factors, such as non-photochemical quenching (NPQ), the efficiency of photochemistry and the three-dimensional structure of the leaf. Hence, F_v/F_m might be determined not only by the loss of the PSII core function but also by other dissipating processes (Malnoë, 2018). Moreover, also theoretical studies have suggested an inherently nonlinear relationship between inactive PSII and the fluorescence signal (Giersch and Krause, 1991).

Over the last decades, various mathematical models of photosynthesis were developed (Stirbet *et al.*, 2020). Some of them focus on the PETC (Zaks *et al.*, 2012; Ebenhöh *et al.*, 2014; Matuszyńska *et al.*, 2016) or the CBB cycle (Pettersson and Ryde-Pettersson, 1988; Poolman *et al.*, 2000), and others try to integrate both into one mathematical description (Morales *et al.*, 2018; Matuszyńska *et al.*, 2019; Saadat *et al.*, 2021). Other models focused on detailed processes in PSII (Belyaeva *et al.*, 2016). Many of these models calculate how the fluorescence signal derives from the molecular processes of the PETC. Most of the calculations depend on equations that describe the fluorescence yield associated with closed and open reaction centres of PSII. The difference in how these models determine fluorescence yield primarily arises from different simplified or extended versions of these equations. These equations are based on the current understanding regarding the source of the fluorescence signal, derived from the work conducted during the last 60 years (Joliot, 1964; Butler and Kitajima, 1975; Kitajima and Butler, 1975; Giersch and Krause, 1991; Bernhardt and Trissl, 1999). However, despite much effort, it still needs to be clarified which of the classical equations and which model representation of the thylakoid membrane (e.g. lake, single unit, domain model, see Bernhardt and Trissl, 1999) is most realistic.

Here, we expanded a published model of the PETC and NPQ (Ebenhöh *et al.*, 2014; Matuszyńska *et al.*, 2016; Saadat *et al.*, 2021) by integrating a mechanistic description of photoinhibition and the D1 repair cycle. For this, we build upon previous models of the D1 damage–repair cycle and an expansion of the energy transfer theory (Giersch and Krause, 1991; Tyystjärvi *et al.*, 1994; Patsikka *et al.*, 1998). The goal of our model is to quantitatively reproduce experimental data measuring photodamage as changes in F_v/F_m, F_m and F_o in wildtype *Arabidopsis thaliana* and the *npq1* mutant. The *npq1* mutant lacks violaxanthin de-epoxidase and, thus, zeaxanthin. Zeaxanthin has been shown to play a critical role in the induction of short-term (qE) and long-term (qZ) quenching processes, potentially protecting against high light-induced damage (Horton *et al.*, 2008; Nilkens *et al.*, 2010). Our model provides a theoretical framework in which we discuss different formulations for the fluorescence yield based on previous work and assess how these agree with experimental data. In particular, we focus on the effects of different heat dissipation capabilities and quenching activities on the fluorescence signal under photoinhibtory conditions. This work helps to clarify which processes contribute to the dynamic changes of photosynthesis under high-light stress. Moreover, we provide a quantitative and mechanistic explanation of the observed changes in the maximum quantum yield of PSII (F_v/F_m), the minimal fluorescence (F_o) and the maximal fluorescence (F_m) after dark-adaption during high light-induced photoinhibition.

2. METHODS

A mathematical model was developed that combines NPQ, the D1 protein repair cycle, and the main protein complexes in the PETC. The model is based on published mathematical descriptions that successfully simulated experimental data in the past (Tyystjärvi *et al.*, 1994; Ebenhöh *et al.*, 2014; Matuszyńska *et al.*, 2016). Most parameter values were obtained from the literature. The model was tested against published data from various plant species and experimentally measured F_v/F_m values (*A. thaliana* ecotype Columbia-0 and the *npq1* mutant).

2.1. Experimental approach

Arabidopsis thaliana (Columbia-0 and *npq1*) seeds were sown on commercial soil (Pikier, Balster Einheitserdewerk, Fröndenberg, Germany) and stratified for 3 days in the dark at 4 °C. After that, they were transferred to the climate chamber with 12 h/12 h light/dark photoperiod, 26 °C/20 °C day/night air temperature and 60 % relative air humidity. The photosynthetically active radiation was provided by fluorescent lamps (Fluora L58 W/77; Osram, Munich, Germany) with an intensity of approximately 100 μmol m^{-2} s^{-1}at plant height. Finally, seedlings were transferred to pots (7 × 7 × 8 cm, one plant per pot) filled with soil (Lignostrat Dachgarten extensive, HAWITA, Vechta, Germany). Care was taken to avoid soil drying during cultivation. Six to seven weeks old plants were used for measuring.

Leaves of *A. thaliana* plants were detached, and petioles were submerged in a 5 mM lincomycin solution in reaction tubes for 3 h in dim light under ventilation. After incubation in the lincomycin solution, leaf discs with a diameter of 1.1 cm were punched out and floated on a water bath to keep the leaf temperature constant at 20 °C. The floating leaf discs were exposed to white LED light (SL 3500-W-G, Photon Systems Instruments) with an intensity of 800 μmol m^{-2} s^{-1}. After 0 h, 0.5 h, 1 h, 3 h, 5 h, and 6 h, F_v/F_m was measured on six replicate leaf discs using

a DUAL-KLAS-NIR system (Heinz Walz GmbH, Effeltrich, Germany). Each leaf was dark-adapted 20 min before a red saturation pulse (635 nm, 0.8 s) of >10 000 μmol m^{-2} $s^{-1}$was applied from both upper and lower sides of the leaf. Fluorescence was detected on the lower leaf surface to determine F_m.

2.2. Model description

Simulations were based on previous models of photosynthesis (Ebenhöh *et al.*, 2014; Matuszyńska *et al.*, 2016) and the D1 protein repair cycle. For a detailed explanation, see the supplement. The photosynthetic electron transport chain in the thylakoid membrane of chloroplasts is implemented according to Ebenhöh *et al.* (2014). A four-state PSII description (B_0—open and non-excited, B_1—open and excited, B_2—closed and non-excited, B_3—closed and excited) was used. The rate of cytochrome b_6f complex is described via mass-action kinetics. Photosystem I (PSI) is a three-state system similar to PSII. Convenience kinetics describes the activities of the ferredoxin-NADPH-reductase (Liebermeister and Klipp, 2006). The proton leak across the thylakoid membrane, ATP synthesis and cyclic electron flow around PSI are modeled via mass action kinetics. Reversible reactions are included by calculating lumenal pH-dependent equilibrium constants. Similar to Matuszyńska *et al.* (2019) and Saadat *et al.* (2021), a four-state quencher module, based on the xanthophyll cycle and the protonation of PsbS, was integrated (see Fig. 1). The model is detailed in the supplementary material.

2.3. D1 protein repair cycle and fluorescence

The repair and synthesis of the D1 protein of PSII were implemented by first-order equations governing the dynamics of three states of PSII (Tyystjärvi *et al.*, 1994). These are PSII with intact D1 protein (U_a), PSII with damaged D1 protein (U_i) and PSII without D1 protein (U_d). Here, $U_a = \sum_{i=1\ldots4} B_i$ comprises the four states of the model without photoinhibition. ATP concentration is denoted as (A).

$$\frac{dU_a}{dt} = k_{REP} \cdot \frac{A}{A + K_{m,pi}} \cdot U_d - (B_1 + B_3) \cdot k_{PI0} \quad (1)$$

$$\frac{dU_i}{dt} = (B_1 + B_3) \cdot k_{PI0} - k_{DEG} \cdot \frac{A}{A + K_{m,pi}} \cdot U_i \quad (2)$$

$$\frac{dU_d}{dt} = k_{DEG} \cdot \frac{A}{A + K_{m,pi}} \cdot U_i - k_{REP} \cdot \frac{A}{A + K_{m,pi}} \cdot U_d, \quad (3)$$

Here, k_{REP} and k_{DEG} are the rate constants for the insertion of newly synthesized and degradation of damaged D1 protein. k_{PI0} is the rate constant of photoinhibition. Several studies indicate that photoinhibition is a costly, energy-consuming process (Raven *et al.*, 2011; Murata and Nishiyama, 2018). Hence, degradation and insertion (PSII repair) of the D1 protein depends on the ATP concentration, implemented via a saturating function (Michaelis–Menten type function).

2.4. Fluorescence

We assume inactive PSII can dissipate excitation energy as heat and emit fluorescence. The fluorescence emitted by these PSII states is still affected by quenching.

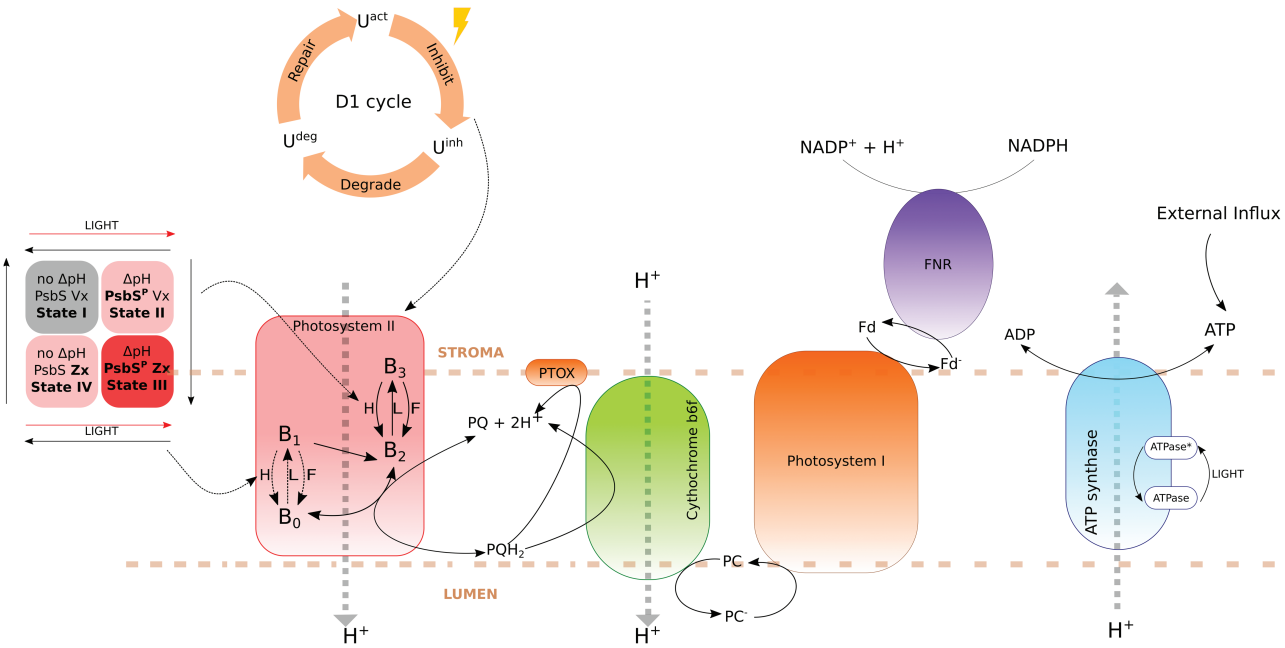

Figure 1. Schematic depiction of the model of photoinhibition (compare also Ebenhöh *et al.*, 2014; Matuszyńska *et al.*, 2016). B_0 and B_1 denote non-excited and excited open photosystem II (PSII). B_2 and B_3 denote non-excited and excited closed PSII. Not shown for clarity but included are the cyclic electron flows around photosystem I.

2.4.1. Isolated PSII

Assuming no energy transfer between active and inactive PSII, the yield of fluorescence is described as (see Giersch and Krause, 1991; Ebenhöh *et al.*, 2014),

$$F = \frac{k_F}{k_F + k_H \cdot Q + k_P} \cdot B_0 + \frac{k_F}{k_F + k_H \cdot Q} \cdot B_2 + \frac{k_F}{k_F \cdot + \rho \cdot k_H \cdot Q} \cdot (U_\mathrm{i} + U_\mathrm{d}), \quad (4)$$

Here, k_F, k_P and k_H are the rate constant of fluorescence, photochemistry and dissipitation of light energy, respectively, other than fluorescence and photochemistry. B_0 and B_2 are open and closed states of active PSII (U_a). The parameter ρ has been introduced to account for different heat dissipation properties between active and inactive PSII. Specifically, it describes the ratio of energy dissipation rates as the heat between inactive ($U_i + U_d$) and active (U_a) states of PSII. Q is the quencher activity.

Minimal fluorescence (F_o) is observed in a dark-adapted state, where $B_0 \approx U_a$. Thus,

$$F_o = \frac{k_F}{k_F + k_H \cdot Q + k_P} \cdot U_a + \frac{k_F}{k_F + \rho \cdot k_H \cdot Q} \cdot (U_\mathrm{i} + U_\mathrm{d}). \quad (5)$$

Assuming there are no inactive photosystems, Equation (5) becomes,

$$F_{o,a} = \frac{k_F}{k_F + k_H \cdot Q + k_P} \cdot \mathrm{PSII}^\mathrm{tot}. \quad (6)$$

This is the expected F_o signal at the beginning of an experiment before high-light treatment starts.

The maximal fluorescence yield is obtained in saturating light conditions, where $B_2 \approx U_a$. Therefore,

$$F_m = \frac{k_F}{k_F + k_H \cdot Q} \cdot U_a + \frac{k_F}{k_F + \rho \cdot k_H \cdot Q} \cdot (U_\mathrm{i} + U_\mathrm{d}), \quad (7)$$

and without inactive PSII, representing the signal at the beginning of high-light treatment,

$$F_{m,a} = \frac{k_F}{k_F + k_H \cdot Q} \cdot \mathrm{PSII}^\mathrm{tot}. \quad (8)$$

To quantify the response of F_o and F_m to high-light stress, we determine the derivatives of the relative fluorescence signals with respect to the active reaction centres, U_a. The non-inhibited state corresponds to $U_a = \mathrm{PSII}^\mathrm{tot}$. We define

$$\varphi_o := \frac{d}{dU_a}\left(\frac{F_o}{F_{o,a}}\right) = \frac{Q \cdot k_H(\rho - 1) - k_P}{\mathrm{PSII}^\mathrm{tot}(Q \cdot k_H \cdot \rho + k_F)}, \quad (9)$$

and

$$\varphi_m := \frac{d}{dU_a}\left(\frac{F_m}{F_{m,a}}\right) = \frac{Q \cdot k_H(\rho - 1)}{\mathrm{PSII}^\mathrm{tot}(Q \cdot k_H \cdot \rho + k_F)}, \quad (10)$$

and the ratio of these two values,

$$\gamma := \frac{\varphi_o}{\varphi_m} = \frac{Q \cdot k_H(\rho - 1) - k_P}{Q \cdot k_H(\rho - 1)}. \quad (11)$$

For a non-photoinhibited state, we get with Equations (6) and (8)

$$\frac{F_v}{F_m} = 1 - \frac{F_o}{F_m} = 1 - \frac{k_F + k_H \cdot Q}{k_F + k_H \cdot Q + k_P} = \frac{k_P}{k_F + k_H \cdot Q + k_P}, \quad (12)$$

and, likewise using Equations (5) and (7), for a photoinhibited state

$$\left(\frac{F_v}{F_m}\right)^i = U_a \cdot \frac{F_v}{F_m} \cdot \frac{k_H \cdot Q \cdot \rho + k_F}{U_a \cdot k_H \cdot Q \cdot (\rho - 1) + \mathrm{PSII}^\mathrm{tot}(k_H \cdot Q + k_F)}. \quad (13)$$

Equation (13) becomes Equation (12) when $U_a = \mathrm{PSII}^\mathrm{tot}$.

2.4.2. Connected inactive and active PSII

In a second model, we assume that active closed PSII can transfer excitation energy to damaged PSII (see Giersch and Krause, 1991). We describe this energy transfer rate as a first order process with rate constant k_T. This leads to the following description of the fluorescence signal,

$$F = \frac{k_F}{k_F + k_H \cdot Q + k_P} \cdot B_0 + \frac{k_F}{k_F + k_H \cdot Q + k_T \cdot (U_\mathrm{i} + U_\mathrm{d})} \cdot B_2 + \frac{k_F}{k_F + \rho \cdot k_H \cdot Q} \cdot (U_\mathrm{i} + U_\mathrm{d}). \quad (14)$$

Hence,

$$F_\mathrm{o} = \frac{k_F}{k_F + k_H \cdot Q + k_P} \cdot U_a + \frac{k_F}{k_F + \rho \cdot k_H \cdot Q} \cdot (U_\mathrm{i} + U_\mathrm{d}), \quad (15)$$

and

$$F_\mathrm{m} = \frac{k_F}{k_F + k_H \cdot Q + k_T \cdot (U_i + U_d)} \cdot U_a + \frac{k_F}{k_F + \rho \cdot k_H \cdot Q} \cdot (U_\mathrm{i} + U_\mathrm{d}). \quad (16)$$

The expression for F_m is a rational function of active PSII ($U_i + U_d = \mathrm{PSII}^\mathrm{tot} - U_a$). This function has a singularity at,

$$U_a = \frac{\mathrm{PSII}^\mathrm{tot} k_T + Q k_H + k_F}{k_T}, \quad (17)$$

and extrema at,

$$U_a = \frac{\mathrm{PSII}^\mathrm{tot} k_T + Q k_H + k_F - \sqrt{(Q k_H \rho + k_F)(\mathrm{PSII}^\mathrm{tot} k_T + Q k_H + k_F)}}{k_T} \quad (18)$$

as well as,

$$U_a = \frac{\mathrm{PSII}^\mathrm{tot} k_T + Q k_H + k_F + \sqrt{(Q k_H \rho + k_F)(\mathrm{PSII}^\mathrm{tot} k_T + Q k_H + k_F)}}{k_T} \quad (19)$$

Note that for $k_T = 0$ the expressions for F_m and F_o are identical to the isolated case. Using Equations (15) and (16), we can derive an expression for F_v/F_m,

$$\left(\frac{F_v}{F_m}\right)^{i,T} = K \cdot U_a \cdot \left(\frac{F_v}{F_m} - \frac{k_T(\mathrm{PSII}^\mathrm{tot} - U_a)}{k_F + k_H \cdot Q + k_P}\right), \quad (20)$$

where

$$K = \frac{k_H \cdot Q \cdot \rho + k_F}{U_a(k_F + k_H \cdot Q \cdot \rho) + (\mathrm{PSII}^\mathrm{tot} - U_a) \cdot (k_F + k_H \cdot Q + k_T \cdot (\mathrm{PSII}^\mathrm{tot} - Ua))}. \quad (21)$$

For $k_T = 0$ Equation (20) becomes identical to Equation (13).

We also tested a model including a forward and backward energy transfer between active and damaged PSII (see Supporting Information) but decided to use the model described above as it is more parsimonious and reasonably explains the experimental data.

2.5. ATP source

In previous models (Ebenhöh *et al.*, 2014; Matuszyńska *et al.*, 2019), an external influx of ATP into the chloroplast is not included. However, several studies have shown that the metabolism of chloroplasts and mitochondria are interconnected and can influence each other (Hoefnagel *et al.*, 1998; Watanabe *et al.*, 2016; Yamada *et al.*, 2020). We assumed that during light conditions, the external influx of ATP into the chloroplast is negligible, and the activity of the PETC provides all ATP. We model the external influx of ATP as constant flux with a light switch to ensure the resynthesis of the D1 protein in darkness.

$$v_{mito} = k_{mito} \cdot \frac{K_{\mathrm{PFD}}^{nL}}{K_{\mathrm{PFD}}^{nL} + \mathrm{PFD}^{nL}}, \tag{22}$$

where k_{mito} is the maximal external influx of ATP, K_{PFD} is the light intensity in which the influx is reduced to 50%, nL is a Hill-type coefficient and PFD is the light intensity.

2.6. Computational analysis

The model was implemented in the Python-based software `modelbase` (version 1.3.8) van Aalst *et al.* (2021). For simulations, the cvode solver implemented in Assimulo (Andersson *et al.*, 2015) was used. Python files containing the model and analyses can be found in the Gitlab repository https://gitlab.com/qtb-hhu/models/2023-photoinhibition.

3. RESULTS

For our analysis, we constructed a mathematical model that combines the description of the PETC as in (Ebenhöh *et al.*, 2014; Matuszyńska *et al.*, 2016) and the D1 damage-repair cycle from (Tyystjärvi *et al.*, 1994) (for details, see "Methods and Supplement" section). In the following, we describe the development of hypotheses about mechanistic aspects of the fluorescence signal during photoinhibition and compare model predictions with experimental observations. Guided by discrepancies between experiments and simulations, we iteratively refine our hypotheses to arrive at a realistic description of the fluorescence signal.

3.1. Experimental dynamics of fluorescence signals

The data [see **Supporting Information—Fig. S1**] comprises F_v/F_m, $\mathrm{F_m}$ and $\mathrm{F_o}$ measurements for *A. thaliana* wildtype and *npq1* mutant plants for different exposure times to high light and with or without treatment with lincomycin, which inhibits chloroplast protein synthesis and thus the D1 repair (see Section 2). The experimental data suggest that the *npq1* mutant, which lacks violaxanthin de-epoxidase enzyme and thus cannot form zeaxanthin in the so-called xanthophyll cycle, reacts more sensitively to high-light stress in water (control) and lincomycin treatment. **Supporting Information—Fig. S1** shows that the relative reduction of F_m is generally more pronounced than the increase of F_o, indicating F_m to be the main factor determining the changes in F_v/F_m in this experiment. While the differences between the water and lincomycin treatment are clearly discernible for the wildtype and *npq1* mutant in the F_m and F_v/F_m signal, this is not the case for F_o.

3.2. Changes in the $\mathrm{F_v/F_m}$ signal

We started our computational analysis with the most simple assumptions for the model extended with photoinhibition: We assume that (i) the duration and intensity of the high-light treatment determine the amount of inactive PSII; (ii) inactive PSII contributes to fluorescence and has the same quenching properties as active PSII and; (iii) there is no energy transfer between active and inactive reaction centres. With these assumptions, our model of photoinhibition cannot reproduce the experimentally observed data [**see Supporting Information—Fig. S1**]. The increase of F_o with prolonged high-light treatment is much higher than in the experiment, while there is only little or no effect for simulated F_m. Interestingly, the F_v/F_m signal can be described by the model, indicating that the F_v/F_m signal alone does not provide sufficient information to understand the underlying mechanisms.

3.3. Fluorescence signal in photoinhibition

Motivated by this observation, we modified our model similar to Giersch and Krause (1991) by assuming that the fluorescence signal and heat dissipation properties of active and inactive PSII can differ. This means we relax assumption 2 stated above. To quantify the different behaviour, we introduce the parameter ρ as the ratio of heat dissipation rate constants between inactive and active states of PSII – see Equation (4). This means that $\rho = 1$ corresponds to the previous model, $\rho < 1$ denotes a model in which inactive PSII dissipate heat less effectively and thus yield more fluorescence than active PSII, and $\rho > 1$ describes the opposite scenario.

Using Equations (5) and (7), we can predict the qualitative changes of F_m and F_o as a response to photodamage:

$$\rho = \begin{cases} 0 < \rho < 1, & F_m \text{ increases, } F_o \text{ increases,} \\ 1 < \rho < \frac{k_P}{k_H \cdot Q} + 1, & F_m \text{ decreases, } F_o \text{ increases,} \\ \rho > \frac{k_P}{k_H \cdot Q} + 1, & F_m \text{ decreases, } F_o \text{ decreases} \end{cases} \tag{23}$$

An increase or decrease of F_m depends only on whether ρ is larger or smaller than 1. In contrast, the F_o behaviour (increase or decrease) depends not only on the value of ρ but also on the quenching activity Q.

Fig. 2 shows that for the case in which the heat dissipation of active and inactive photosystems is identical ($\rho = 1$, continuous lines), F_v/F_m follows a linear relationship with the fraction of active PSII, both in a low and high quenching scenario (black and red lines). However, the relationship becomes nonlinear when

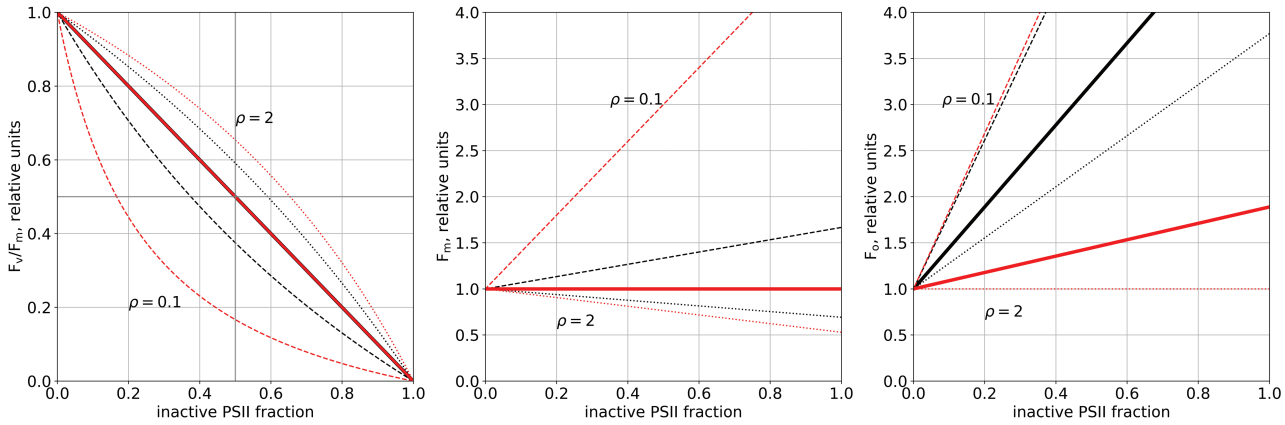

Figure 2. Relationship between F_v/F_m, F_m and F_o and fraction of inactive PSII based on Equation (4). The dashed, continuous and dotted lines indicate scenarios in which the ratio of heat dissipation between inactive and active PSII is 0.1, 1 and 2, respectively. Black lines signify a low quenching, while red lines denote high quenching activity ($Q = 0.1$ and 1). Parameter values used for the calculations can be found in Supporting Information—Table S1. For colour figure refer to online version.

the active and inactive PSII differ in their heat dissipation capabilities. We further observe that ρ determines the curvature of the relationship between F_v/F_m and active PSII fraction, while an active quencher makes the non-linearity more pronounced. The dependence of F_m and F_o on active PSII is linear in all cases. However, the slope is affected both by ρ and Q. Note that F_m is not affected by photoinhibition for $\rho = 1$ (original model, Supporting Information—Fig. S1, see also Giersch and Krause, 1991).

For a fluorescence yield model without energy transfer, the ratio of the slopes of relative values of F_o and F_m as functions of active PSII is given by Equation (11). The slope ratio has a singularity at $\rho = 1$ where the slope of F_m becomes zero. The slope ratio is zero at $\rho = k_P/(k_H \cdot Q)+1$, when the slope of F_o is zero. In our fluorescence measurements for *A. thaliana* during high-light treatment, we observed that the relative increase of F_o is smaller than the relative decrease of F_m. To reproduce this behaviour, the slope ratio must be negative, in the range between -1 and 0. For this, ρ must be constrained to the interval

$$\frac{k_P}{2k_H \cdot Q} + 1 \leq \rho \leq \frac{k_P}{k_H \cdot Q} + 1. \qquad (24)$$

Fig. 3 depicts the slope ratio for the parameter values in the model for two different quenching activities. In a low quenching scenario ($Q = 0.1$, solid line), the parameter ρ is predicted to lie in the range between 6 and 11. This means that, in order to reproduce the experimentally observed slope ratio, damaged PSII needs to dissipate heat at a rate at least six times larger than that at which intact PSII does. Similarly, in a high quenching scenario ($Q = 1$, dotted line) we find $1.5 \leq \rho \leq 2$, which means a one- to twofold faster heat dissipation for damaged versus active PSII.

We used these constraints to fit our model to the experimental data. We find that the data could be considerably better explained than in the model with $\rho = 1$ [**see Supporting Information—Figs. S2 and S3**]. With the parameter ρ in the range determined above, all qualitative features of the fluorescence traces could be reproduced. However, there are still quantitative discrepancies, which could not be resolved using this model.

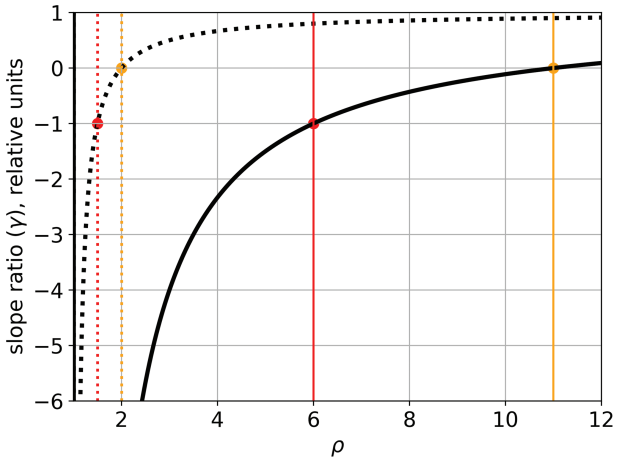

Figure 3. The slope ratio γ for a model without energy transfer in a high (dotted line) and low quenching scenario (continuous line). Vertical lines indicate the points at which the slope ratio is -1 or 0. Parameters are the same as for Fig. 2.

We, therefore, expanded the model to include excitation energy transfer between closed active and damaged PSII, following the example in Giersch and Krause (1991). This leads to a modified formula to describe F_m, whereas the description for F_o remains the same as in the case without energy transfer (see Equations (15) and (16). Consequently, the relation between F_m and active PSII becomes nonlinear (see Fig. 4). The effect of an excitation energy transfer between active and inactive PSII leads to a faster decrease of the F_v/F_m value in response to lowering the active PSII fraction. Moreover, the effect of the energy transfer seems to be larger in a low quenching than a high quenching state (compare Figs. 2 and 4). Because the description of F_o does not change compared to the isolated case, ρ and the quencher activity are still the determining factor for the behaviour of F_o. However, the behaviour of F_m is a nonlinear function of the active PSII fraction, and, therefore, a slope ratio can no longer be uniquely defined.

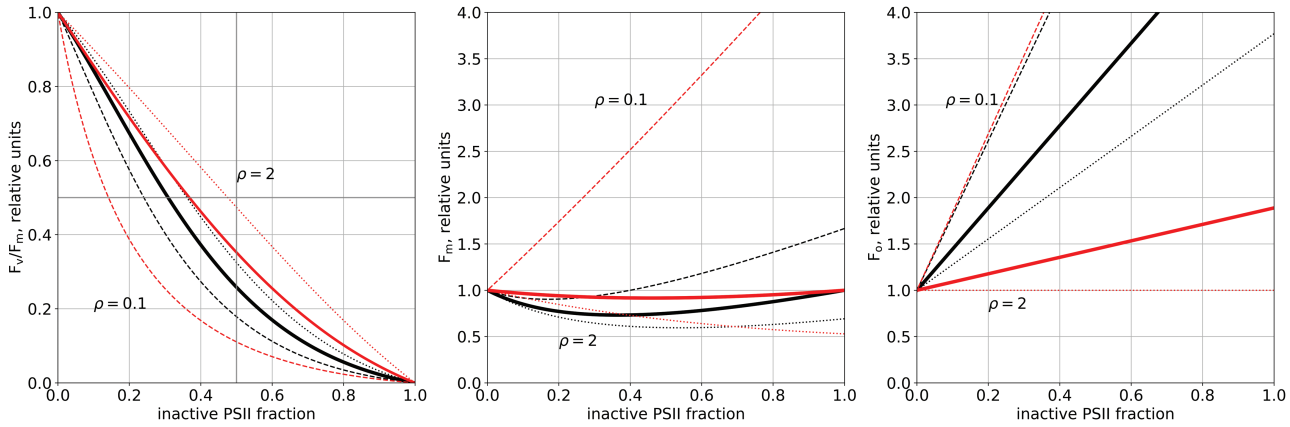

Figure 4. Relationship between F_v/F_m, F_m and F_o and a fraction of inactive PSII based on Equation (14). The dashed, continuous and dotted lines indicate scenarios in which the ratio of heat dissipation between inactive and active PSII is 0.1, 1 and 2, respectively. Black lines signify a low quenching, while red lines denote high quenching activity ($Q = 0.1$ and 1). Parameter values used for the calculations can be found in the Supporting Information—Table S1. Energy transfer was set to 9×10^8 mmol^{-1} (mol Chl) s^{-1}. For colour figure refer to online version.

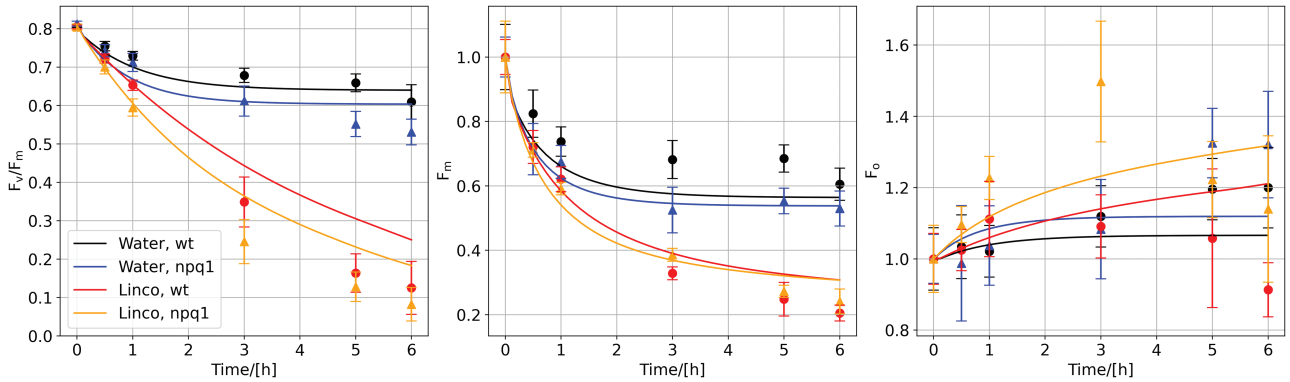

Figure 5. Experimental measurement and simulated changes in F_v/F_m, F_m and F_o in high-light treatment of *A.thaliana* plants for 6 h. The plants were either treated with water (black and blue lines) or lincomycin (red and orange lines) inhibiting protein synthesis. Light intensity was 800 µmol m^{-2} s^{-1}. For colour figure refer to online version.

3.4. Model predictions

Guided by comparison of model predictions and experimental data, we have iteratively refined a model of the photosynthetic electron transport chain. The resulting model includes the assumption that energy quenching differs between active and damaged photosystems. However, energy can be transferred from active to damaged photosystems. This model version can satisfactorily reproduce our experimental data for *A. thaliana* (see Fig. 5, the residuals defined as sum of the squared difference between experimental data points and simulation decreased from 58.82 to 0.58 in comparison to our initial model version). In the following, we employ our model to make novel predictions of how photoinhibition affects key photosynthetic parameters.

3.4.1. *Quenching shifts the fraction of closed and open PSII during photoinhibition*

To describe the internal processes of PSII, we used a simplified mathematical representation that has been applied successfully for modeling fluorescence signal changes in connection to state transition and NPQ (Ebenhöh *et al.*, 2014; Matuszyńska *et al.*, 2016, 2019). This representation of PSII can be approximated by a two-state system consisting of the open and closed active PSII states.

Fig. 6 shows the changes of closed and open active PSII states during exposure to various light intensities for 4 h as phase-space trajectories. We investigate four model versions with (left column) and without (right column) dynamic quencher activity as well as with non-constantly (top row) and constantly active (bottom row) ATP synthase. The version with non-constantly active ATP synthase and dynamic quencher is our original model (top left). For all four versions, the phase-space provides information about the different stages we observe during the onset of photoinhibition. These stages are characterized by the different time-scales on which they operate. The simulation starts with a dark-adapted state and, hence, with no closed PSII. When the light is switched on, the system almost instantaneously changes to a state where both closed, and open PSII are present. The ratio of open to closed PSII depends on the light intensity. A light intensity of around 1000 µmol m^{-2} s^{-1}results in approximately

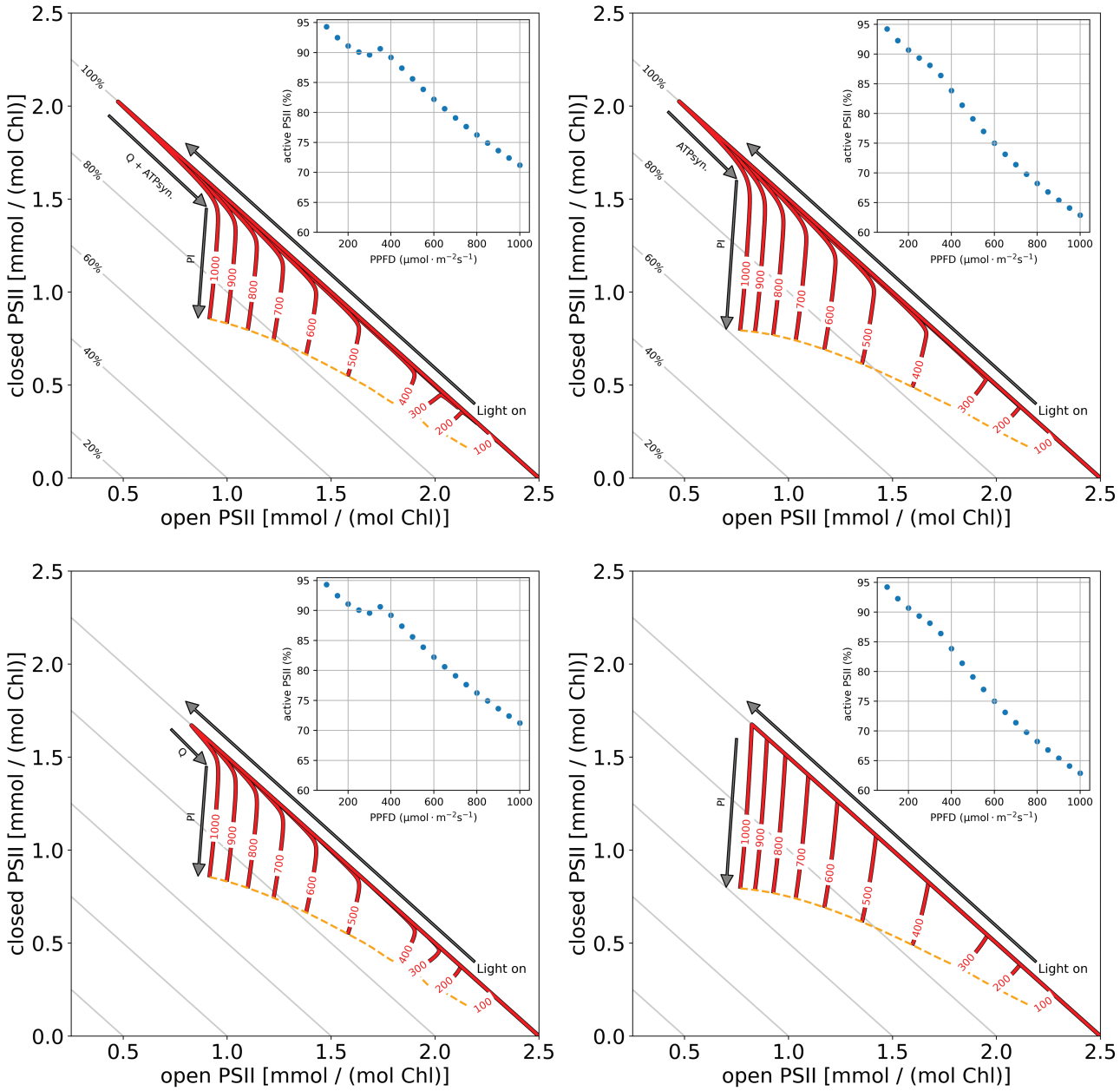

Figure 6. Phase-space of open (B_0) and closed (B_2) active PSII states during photoinhibtory treatment in various light intensities (100 — 1000 µmol m^{-2} s^{-1}). Red lines indicate changes in open and closed PSII. The orange dashed line connects all points in the phase-space reached after 4 h of light treatment. Grey lines indicate the fraction of total active PSII. The inset shows the fraction of active PSII as a function of applied light intensity at the end of the simulation. The top left and top right panels show the phase-space of a model version with and without a dynamic quencher. The bottom left and bottom right show the phase-space of a model version with and without a dynamic quencher and without ATP synthase activation. For colour figure refer to online version.

85 % of PSII in the closed state. This initial stage is driven by the rapid processes in PSII.

The first stage is followed by the second stage, which operates on a time-scale of seconds to minutes. In this phase, two effects dominate. First, ATP synthase is activated (arrows marked as "Q + ATPsyn." and "ATPsyn"). Second, the fast component of the quencher is rapidly activated, leading to a slower activation of PSII and thus a smaller fraction of closed states (compare the top row with the bottom row). Comparing the left (dynamic quencher) and right (no quencher) columns as well as the top (non-constantly active ATP synthase) and bottom (constantly active ATP synthase) rows of Fig. 6 illustrates the effect of these two processes individually. In this stage, photoinhibition starts to become active but photodamage is still negligible.

This stage is followed by the slower stage of photoinhibition, which extends over several hours. Here, the active amount of PSII is gradually reduced due to photodamage. In the phase-space this is reflected by the downward pointing red lines. This

phase continues until repair processes compensate for the extent of the light-induced damage, indicated by the dashed yellow lines. By comparing the four model versions with and without a dynamic quencher and with non-constantly and constantly active ATP synthase, it becomes apparent that quenching not only leads to more open PSII but also reduces the extent of photodamage, visible by the shorter downward trajectories for the model with active quencher. In our model simulation and with our chosen parameters, the quenching activity leads to almost 10 % more active PSII after 4 h of light treatment with an intensity of 1000 μmol m^{-2} s^{-1} (see inset in Fig. 6).

3.4.2. *Steady-state photoinhibition analysis*

We observed that dynamic quenching, associated with PsbS, a subunit of PSII that is involved in NPQ, and the xanthophyll cycle (Fig. 5), is a key determinant for the extent of high-light stress-induced photodamage. We employed our model to systematically analyse the connection between quenching and the steady-state behavior for different light intensities. For this, rate constants associated with NPQ were set to zero and the quenching activity was fixed to be a constant value. Subsequently, the system was simulated until it reached a steady state. Fig. 7 displays the computed steady-state photoinhibition rate.

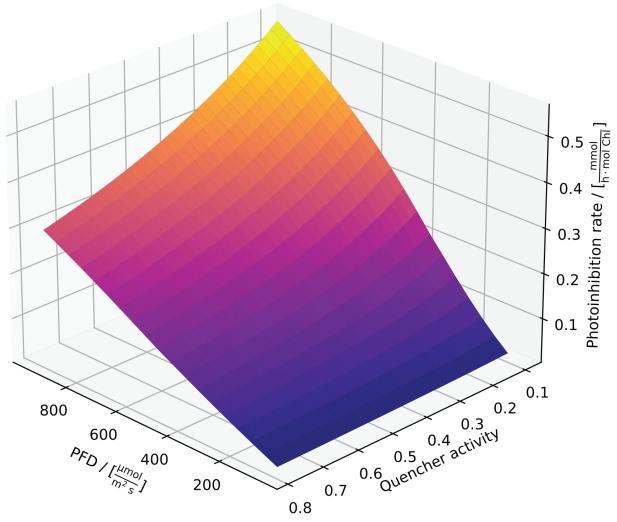

Figure 7. The predicted stationary flux of photoinhibition for different light intensities and different quencher activities. Quenching activities were modeled for these predictions by imposing fixed values (*x*-axis) between 0.1, representing almost no quencher activity, and 0.8, representing double the quencher activity typically observed in our model simulations. Light intensity (*y*-axis) was varied. The system was simulated for each combination of light intensity and quenching activity until a steady state was reached. On the *z*-axis, the stationary photoinhibition rate is plotted. For low quenching activities, a sigmoidal transition between high and low photoinhibition rates is observed with light intensities. This demonstrates that small light intensity changes can already have strong photoinhibitory effects in low light regimes. For higher quenching activities, the transition is smoother, almost linear, indicating higher flexibility, as expected, more flexibility against high-light stress.

In low quenching regimes, we observe a slightly sigmoidal transition between high and low photoinhibition rates with increasing light intensities. For very low quenching activities, the photoinhibition rate increases quickly, having a disproportionally high increase at around 400 μmol m^{-2} s^{-1}. This demonstrates that small light intensity changes can already have strong photoinhibitory effects in low light regimes. By contrast, when quenching is active, we observe a smooth transition from low to high-light intensities, indicating greater tolerance against high-light stress.

4. DISCUSSION AND CONCLUSIONS

We have presented a model of the PETC integrating NPQ and photoinhibitory processes. The model aims to (i) investigate how fluorescence signals (F_m and F_o) in response to photoinhibition can be explained, (ii) explore which assumptions are sufficient to reproduce experimental data, (iii) study the effects of different modes of energy quenching and (iv) quantify stationary photoinhibtory rates. To do so, we followed a reductionist approach. Our initial model version of photodamage in the PETC was built on the simple assumptions that (i) photoinhibition is proportional to the intensity and duration of light treatment, (ii) there is no difference between heat dissipation properties of active and damaged photosystems, and (iii) there is no energy transfer between photosystems. However, this version could not reproduce the experimental data [**see Supporting Information—Fig. S1**]. Motivated by differences between simulations and experimental data, we systematically increased the complexity of the model representation by firstly introducing differences in heat dissipation properties of active and inactive photosystems (Fig. 2) and secondly an energy transfer between closed active and inactive photosystems in the description of the fluorescence signal (Fig. 4).

Both additions are realistic and have previously been used to study fluorescence changes after high-light treatment (Giersch and Krause, 1991) with fluorescence yield models. This previous investigation did not include a dynamic lumenal pH-induced quenching component. Our model implements quenching based on the four-state model introduced by Horton *et al.* (2008), which is also included in Matuszyńska *et al.* (2016). In comparison to Matuszyńska *et al.* (2016), in our model version, the influence of the qZ component (zeaxanthin concentration high, no PsbS protonation) is reduced. This modification was necessary to realistically simulate differences between the wild type and *npq1* mutant. After introducing all these changes to our initial model version, the fit agreed with experimental data (Fig. 5), supporting the assumptions that heat dissipation properties differ between intact and damaged photosystems and that energy transfer occurs.

Whereas the F_v/F_m and F_m signals could be reproduced with deviations in the range of experimental errors in many parts of their experimental traces, the experimental F_o signal deviates from our simulated fluorescence traces. We hypothesized that a long-term quencher independent of the xanthophyll cycle and PsbS protonation, not yet implemented, could improve the model fit. To test this, we implemented an additional component

in the quencher description of Matuszyńska *et al.* (2016) proportional to inactive PSII to our first model version (without heat dissipation differences and energy transfer). This should mimic a quenching process proportional to high-light stress that is still strongly active after dark adaption. Although the changes in the F_m, F_v/F_m and F_o signal are now primarily products of the long-term quencher (compare **Supporting Information—Fig. S1** and **Supporting Information—Fig. S4**), the agreement between simulated and experimental fluorescence traces improved, even reproducing the decrease of the F_o signal in lincomycin treatment [**see Supporting Information—Fig. S4**]. This additional quenching component would lead to increased quenching activity and eventually to an even lower rate of photoinhibition than predicted by our standard model (compare Fig. 7). However, the conditions under which we recorded the experimental data should not induce any additional strong long-term quenching component, motivating us to discard this long-term quencher hypothesis and instead focus on the initial simple description of fluorescence yield based on Giersch and Krause (1991).

Although the model can reproduce the F_v/F_m and F_m signals in many parts, limitations still need to be discussed. Firstly, the simulated wild-type F_m values depart from measured values, especially in the later phases of the fluorescence spectroscopic experiment (compare Fig. 5), while the *npq1* mutant values are better described. This deviation in WT indicates that the model still needs to be improved. Because the F_m value is influenced by the amount of damaged PSII and long-term quenching components, the differences between measured and simulated values suggest that we overestimate at least one of these processes. We hypothesize that not-yet-implemented regulatory mechanisms could lead to a better agreement between simulation and experiment. There is evidence that regulation of the D1 protein repair cycle dynamics and qE might play a pivotal role in processes connected to photoinhibition (Bethmann *et al.*, 2019; Chotewutmontri and Barkan, 2020). However, we have restrained so far in their implementation because their exact mechanisms are still under investigation, and clear parameter values needed for their *in silico* representation are hard to find. Secondly, it seems to be the case that our model predicts a steady state too early when looking at the simulated F_v/F_mtraces (see Fig. 5). This is due to the early saturation of the simulated F_o values. As indicated previously, F_o replication is one of the main limitations of our model. Because the F_v/F_m signal is derived from F_m and F_o, we hypothesize that an improved representation of F_o would lead to more realistic dynamics of F_v/F_m. However, it remains difficult to pinpoint what is missing in the model because similar processes in and around the thylakoid membrane influence all investigated signals (F_m, F_o, F_v/F_m), and the signals are, to a certain degree, interdependent.

Besides replicating experimental data, the value of a model lies in providing a way to investigate biological phenomena not easily accessible by experiments. Here, we specifically focused on the changes in excited and non-excited active PSII during photoinhibition. We used a phase-space visualization to observe the dynamic response of the system to different light conditions (Fig. 6). Our results show that one effect of the quencher is to actively push PSII to more open states, leading to a long-term reduction of high-light-induced photodamage. The changes in active PSII shown in Fig. 6 is probably due to the activation of the ATP synthase and the saturation of the quencher. Additionally, we investigated the effects of quenching for steady-state rates of photodamage and found a disproportionally strong effect of high-light stress in low-quenching scenarios (Fig. 6). In high-quenching scenarios, the response becomes linear, indicating that quenching might be essential for the flexible behaviour of photosynthetic organisms under high-light stress.

Combining the previous observations, we might speculate that fluorescence changes induced by high-light stress are caused by a combination of various processes, including the reduction of PSII core functionality and multiple long- and short-term quenching mechanisms. Our simulations indicate that to explain observed changes in the F_v/F_m, F_m and F_o signals, three components are essential: (i) the amount of active and inactive PSII, (ii) the difference between their heat dissipation properties and (iii) quenching phenomena. For the latter, it is essential to distinguish between short- and long-lived quencher components. While short-lived quenchers influence the decrease of the active PSII fraction but not the fluorescence signal measured after dark-adaption, long-lived quenchers influence both.

There is a continuous discussion about whether inactive PSII is photoprotective (Matsubara and Chow, 2004; Sarvikas *et al.*, 2010; Kou *et al.*, 2012). This hypothesis was based on the observation that an active PSII pool remained even after prolonged high-light treatment and repair inhibited by lincomycin (Lee *et al.*, 2001). However, later studies did not support these findings and it was speculated that the observed active pools resulted from the specific experimental setup (Kou *et al.*, 2012). Regarding the mechanism, it was hypothesized that photoprotection is caused by an energy transfer from active to inactive photosystems, which are more efficient energy quenchers (Matsubara and Chow, 2004). It was argued that without energy transfer photoinhibition is a first-order process and that the existence of an energy transfer and photoprotection should be detectable by a deviation from an exponential kinetics (Matsubara and Chow, 2004; Sarvikas *et al.*, 2010).

With our model, we can test these hypotheses by simulating the respective scenarios. **Supporting Information—Fig. S5** shows the dynamics of PSII simulated with (red) and without (orange) assumed energy transfer. We observe that in both cases the dynamics of active PSII closely resemble a simple exponential, and thus may be interpreted as a first-order process. However, even in the case without energy transfer, small discrepancies from the exponential behaviour are visible. Although such small differences are unlikely to be experimentally detectable, they can be theoretically explained. An exact exponential decay would entail that the fraction of excited PSII (relative to active PSII) remains constant. However, in our simulations, this is not precisely the case [see **Supporting Information—Fig. S6**]. The cause for this is that the redox state of the plastoquinone pool and the state of the quencher depend on the rate of electrons provided by PSII, and thus on the amount of active PSII itself, leading to a non-trivial dynamics which is only approximately exponential. Interestingly, even the decay of PSII under the assumption of energy transfer closely resembles an exponential.

We, therefore, conclude that observing discrepancies from an exponential behaviour might not be the best-suited method to discriminate between the two hypotheses.

This is especially the case when using F_v/F_m as a measure of photoinhibition. Our calculations have shown that, in a scenario without energy transfer, changes in F_v/F_m only follow the active PSII decay proportionally if the active and inactive PSII have identical heat dissipation properties ($\rho = 1$, see Fig. 2). However, because we used F_m and F_o, besides F_v/F_m, to guide our simulations, we could show that the experimental observations can only be explained if $\rho > 1$, which means that inactive PSII quench energy more efficiently than active PSII. This, in turn, means that F_v/F_m is a nonlinear function of inactive PSII, and as a consequence, the F_v/F_m signal displays a slightly different kinetic than the active PSII pool [see **Supporting Information—Figs. S5 and S7**]. Nonetheless, without energy transfer a value of $\rho > 1$ results in a simulated F_v/F_m that is too large compared to the experiment [see **Supporting Information—Figs. S2 and S3**]. Assuming an energy transfer leads to reduced simulated F_v/F_m values and allows quantitative reproduction of the measured signal (Figs. 4 and 5). Interestingly, energy transfer leads to a more linear response of the F_v/F_m signal to inactive/active PSII [**Supporting Information—see Fig. S7**], resulting in a F_v/F_m dynamics that follows the response of the approximately simulated exponential decay of PSII more closely. Thus, our theoretical analysis allowed discrimination between the effects of higher energy quenching of inactive PSII and energy transfer. Our results support the existence of energy transfer processes from active to inactive PSII.

In conclusion, we used a mathematical model of the PETC to investigate the fluorescence signal during photoinhibition and identified key factors that need to be included in order to realistically explain experimental fluorescence data. In addition to the hypotheses explored in this work, there are many other conceivable extensions and improvements. One possible extension is to include PSI fluorescence, as was done in Stirbet and Govindjee (2016). We speculate that the PSI contribution might lead to a more realistic reproduction of the F_o signal. In addition, it may become important to include a description of PSII heterogeneity. The PSII pool consists of so-called PSIIα and PSIIβ complexes. Both differ in their antenna size and localization in the thylakoid membrane (Melis, 1985; Black *et al.*, 1986). In preliminary investigations, we found that including such a heterogeneity does not change the slope ratio as defined in Equation (11), which is a key indicator for the model response [see Supporting Information]. However, a full and realistic implementation of PSIIα and PSIIβ and their different properties into our dynamic model is a future project. So far, also spatial effects have been ignored, in order to reduce the complexity of the *in silico* analysis. However, considering the complex three-dimensional structure of thylakoid membranes, these may be important to consider for more realistic models (Kirchhoff, 2013). Additionally, it has been shown that the spatial architecture of leaves and the place of measurement (ad-, abaxial or within leaves) influence the fluorescence signal obtained by spectroscopic techniques during photoinhibition (Oguchi *et al.*, 2011). Because we used a Dual-KLAS-NIR device for our measurements that records fluorescence on the abaxial leaf surface, future model versions should account for different local origins of the fluorescence signal. This is because the changes in the fluorescence signal obtained by devices measuring the abaxial surface, such as a Dual-KLAS-NIR, might correlate more with changes in chloroplasts in the lower than in the upper layers of the leaf. We envisage that our model can be used as a platform for the investigation of photoinhbitory effects, with several applications in mind. These include the study of long-term extinction phenomena (qZ and qH), which could support experimental efforts to identify the molecular mechanisms responsible for such quenching phenomena (Malnoë, 2018). For instance, the model can be used to quantify the contribution of different quenching mechanisms during high-light treatment by fitting the simulated fluorescence signals to experimental measurements. Analysing the necessary parameter changes for achieving agreement between simulation and experiment allows hypothesizing which molecular processes are most relevant for high-light protection in different environmental conditions. Moreover, our model also opens the possibility of investigating evolutionary questions. For example, by modifying the appropriate parameters, it can be used to explore the quenching capacities of a wide range of plant and algal species, thus supporting the generation of hypotheses explaining the enormous natural variation found in photoprotective processes (Matuszyńska *et al.*, 2016; Rungrat *et al.*, 2019).

SUPPORTING INFORMATION

The following additional information is available in the online version of this article –

Table S1. Parameter values.
Figure S1. Experimental and simulated changes in F_v/F_m, F_m, and F_o in high light treatment. The model did not assume energy transfer processes and differences in heat dissipation properties between active and inactive PSII.
Figure S2. Experimental and simulated changes in F_v/F_m, F_m, and F_o in high light treatment. The model did include differences in heat dissipation properties between active and inactive PSII ($\rho = 6$) and no energy transfer.
Figure S3. Experimental and simulated changes in F_v/F_m, F_m, and F_o in high light treatment. The model did include differences in heat dissipation properties between active and inactive PSII ($\rho = 11$) and no energy transfer.
Figure S4. Experimental and simulated changes in F_v/F_m, F_m, and F_o in high light treatment. The model assumed $\rho = 1$, $kT = 0$, and slow quenching.
Figure S5. Simulated changes in active PSII and F_v/F_m in a model with and without energy transfer between active and inactive PSII.
Figure S6. Simulated changes in excited PSII states (B1 and B3), quencher activity and plastoquinone redox state in a model with and without energy transfer between active and inactive PSII.
Figure S7. Simulated changes in F_v/F_m as function of inactive PSII in a model with and without energy transfer between active and inactive PSII.
Figure S8. Relationship between F_v/F_m, F_o, and F_m and inactive PSII in a model with back and forward energy transfer between inactive and active PSII.

Figure S9. Relationship between F_v/F_m, F_o, and $F_m$and inactive PSII in a model without energy transfer between inactive and active PSII and with PSII heterogeneity.

ACKNOWLEDGMENT

We thank Ana Carolina dos Santos Sá and Yuxi Niu for their help during the experimental measurements.

AUTHOR CONTRIBUTIONS

T.N. and O.E.: initial idea and conceptualization. O.E.: funding acquisition. T.N.: visualisation. T.N.: formal analyses. T.N. and O.E.: writing—original draft and introduction. T.N. and O.E.: writing—original draft and methods. T.N. and O.E.: writing—original draft and results. T.N. and O.E.: writing—original draft, discussion and T.N., O.E. and S.M. writing—review and editing. All authors read and accepted the final version of the manuscript.

CONFLICT OF INTEREST

The authors declare that the research was conducted in the absence of any commercial or financial relationships that could be construed as a potential conflict of interest.

FUNDING

This work was funded by the Deutsche Forschungsgemeinschaft (DFG), project ID 391465903/GRK 2466 (T.N.). O.E. and S.M. were supported by Deutsche Forschungsgemeinschaft under Germany's Excellence Strategy – EXC-2048/1 – project ID 390686111.

DATA AVAILABILITY

The original contributions presented in the study are included in the article/Supplementary Material, further inquiries can be directed to the corresponding author/s. The code can be found at https://gitlab.com/qtb-hhu/models/2023-photoinhibition.

LITERATURE CITED

Andersson C, Claus F, Akesson J. 2015. ScienceDirect Assimulo: a unified framework for ODE solvers. *Mathematics and Computers in Simulation* 116:26–43.

Belyaeva NE, Bulychev AA, Yu Riznichenko G, Rubin AB. 2016. Thylakoid membrane model of the chl a fluorescence transient and p700 induction kinetics in plant leaves. *Photosynthesis Research* 130:491–515.

Bernhardt K, Trissl H-W. 1999. Theories for kinetics and yields of fluorescence and photochemistry: how, if at all, can different models of antenna organization be distinguished experimentally? *Biochimica et Biophysica Acta (BBA)-Bioenergetics* 1409:125–142.

Bethmann S, Melzer M, Schwarz N, Jahns P. 2019. The zeaxanthin epoxidase is degraded along with the D1 protein during photoinhibition of photosystem II. *Plant Direct* 3:1–13.

Black MT, Brearley TH, Horton P. 1986. Heterogeneity in chloroplast photosystem II. *Photosynthesis Research* 8:193–207.

Butler WL, Kitajima M. 1975. Fluorescence quenching in photosystem II of chloroplasts. *Biochimica et Biophysica Acta (BBA)-Bioenergetics* 376:116–125.

Chotewutmontri P, Barkan A. 2020. Light-induced PSBA translation in plants is triggered by photosystem II damage via an assembly-linked autoregulatory circuit. *Proceedings of the National Academy of Sciences* 117:21775–21784.

Ebenhöh O, Fucile F, Finazzi G, Rochaix J-D, Goldschmidt-Clermont M. 2014. Short-term acclimation of the photosynthetic electron transfer chain to changing light: a mathematical model. *Philosophical Transactions of the Royal Society B: Biological Sciences* 369:20130223.

Giersch C, Krause GH. 1991. A simple model relating photoinhibitory fluorescence quenching in chloroplasts to a population of altered photosystem II reaction centers. *Photosynthesis Research* 30: 115–121.

Hoefnagel MHN, Atkin OK, Wiskich JT. 1998. Interdependence between chloroplasts and mitochondria in the light and the dark. *Biochimica et Biophysica Acta (BBA)-Bioenergetics* 1366:235–255.

Horton P, Johnson MP, Perez-Bueno ML, Anett Z Kiss AZ, Ruban AV. 2008. Photosynthetic acclimation: does the dynamic structure and macro-organisation of photosystem II in higher plant grana membranes regulate light harvesting states? *The FEBS Journal* 275:1069–1079.

Joliot P. 1964. Etude cinetique de la reaction photochimique liberant l'oxygene au cours de la photosynthese. *Comptes Rendus de l'Académie des Sciences* 258:4622–4625.

Kaiser E, Morales A, Harbinson J. 2018. Fluctuating light takes crop photosynthesis on a rollercoaster ride. *Plant Physiology* 176:977–989.

Khorobrykh S, Havurinne V, Mattila H, Tyystjärvi E. 2020. Oxygen and ros in photosynthesis. *Plants* 9:91.

Kirchhoff H. 2013. Architectural switches in plant thylakoid membranes. *Photosynthesis Research* 116:481–487.

Kitajima M, Butler WL. 1975. Quenching of chlorophyll fluorescence and primary photochemistry in chloroplasts by dibromothymoquinone. *Biochimica et Biophysica Acta (BBA)-Bioenergetics* 376:105–115.

Kou J, Oguchi R, Fan DY, Chow WS. 2012. The time course of photoinactivation of photosystem II in leaves revisited. *Photosynthesis Research* 113:157–164.

Ksenzhek OS, Volkov AG. 1998. *Plant energetics*. USA: Academic Press.

Lee H-Y, Hong Y-N, Chow WS. 2001. Photoinactivation of photosystem II complexes and photoprotection by non-functional neighbours in *Capsicum annuum* L. leaves. *Planta* 212:332–342.

Li L, Aro E-M, Millar AH. 2018. Mechanisms of photodamage and protein turnover in photoinhibition. *Trends in Plant Science* 23: 667–676.

Liebermeister W, Klipp W. 2006. Bringing metabolic networks to life: convenience rate law and thermodynamic constraints. *Theoretical Biology and Medical Modelling* 3:1–13.

Malnoë A. 2018. Photoinhibition or photoprotection of photosynthesis? Update on the (newly termed) sustained quenching component qh. *Environmental and Experimental Botany* 154:123–133.

Matsubara S, Chow WS. 2004. Populations of photoinactivated photosystem II reaction centers characterized by chlorophyll a fluorescence lifetime *in vivo*. *Proceedings of the National Academy of Sciences* 101:18234–18239.

Matuszyńska A, Heidari S, Jahns P, Ebenhöh O. 2016. A mathematical model of non-photochemical quenching to study short-term light memory in plants. *Biochimica et Biophysica Acta (BBA)-Bioenergetics* 1857:1860–1869.

Matuszyńska A, Saadat NP, Ebenhöh O. 2019. Balancing energy supply during photosynthesis—a theoretical perspective. *Physiologia Plantarum* 166:392–402.

Melis A. 1985. Functional properties of photosystem II β in spinach chloroplasts. *Biochimica et Biophysica Acta (BBA)-Bioenergetics* 808:334–342.

Morales A, Yin X, Harbinson J, Driever SM, Molenaar J, Kramer DM, Struik PC. 2018. In silico analysis of the regulation of the photosynthetic electron transport chain in c3 plants. *Plant Physiology* 176:1247–1261.

Muller P, Li X-P, Niyogi KK. 2001. Non-photochemical quenching: a response to excess light energy. *Plant Physiology* 125:1558–1566.

Murata N, Nishiyama Y. 2018. ATP is a driving force in the repair of photosystem II during photoinhibition. *Plant, Cell & Environment* 41:285–299.

Nies T, van Aalst M, Saadat N, Ebeling J, Ebenhöh O. 2023. What controls carbon sequestration in plants under which conditions? *Biosystems* 231:104968.

Nilkens M, Kress E, Lambrev P, Miloslavina Y, Müller M, Holzwarth AR, Jahns P. 2010. Identification of a slowly inducible zeaxanthin-dependent component of non-photochemical quenching of chlorophyll fluorescence generated under steady-state conditions in arabidopsis. *Biochimica et Biophysica Acta (BBA)-Bioenergetics* 1797: 466–475.

Oguchi R, Douwstra P, Fujita T, Chow WS, Terashima I. 2011. Intra-leaf gradients of photoinhibition induced by different color lights: implications for the dual mechanisms of photoinhibition and for the application of conventional chlorophyll fluorometers. *New Phytologist* 191:146–159.

Patsikka E, Aro E-M, Tyystjarvi E. 1998. Increase in the quantum yield of photoinhibition contributes to copper toxicity *in vivo*. *Plant Physiology* 117:619–627.

Pettersson G, Ryde-Pettersson U. 1988. A mathematical model of the calvin photosynthesis cycle. *European Journal of Biochemistry* 175:661–672.

Poolman MG, Fell DA, Thomas S. 2000. Modelling photosynthesis and its control. *Journal of Experimental Botany* 51:319–328.

Raven JA. 2011. The cost of photoinhibition. *Physiologia Plantarum* 142:87–104.

Rungrat T, Almonte AA, Cheng R, Gollan PJ, Stuart T, Aro E-M, Borevitz JO, Pogson B, Wilson PB. 2019. A genome-wide association study of non-photochemical quenching in response to local seasonal climates in *Arabidopsis thaliana*. *Plant Direct* 3:e00138.

Saadat NP, Nies T, Van Aalst M, Hank B, Demirtas B, Ebenhöh O, Matuszyńska A. 2021. Computational analysis of alternative photosynthetic electron flows linked with oxidative stress. *Frontiers in Plant Science* 12:750580.

Sarvikas P, Tyystjärvi T, Tyystjärvi E. 2010. Kinetics of prolonged photoinhibition revisited: photoinhibited photosystem II centres do not protect the active ones against loss of oxygen evolution. *Photosynthesis Research* 103:7–17.

Stirbet A, Govindjee G. 2016. The slow phase of chlorophyll a fluorescence induction *in silico*: origin of the S–M fluorescence rise. *Photosynthesis Research* 130:193–213.

Stirbet A, Lazár D, Guo Y, Govindjee G. 2020. Photosynthesis: basics, history and modelling. *Annals of Botany* 126:511–537.

Tyystjärvi E, Mäenpää P, Aro E-M. 1994. Mathematical modelling of photoinhibition and photosystem II repair cycle. I. Photoinhibition and d1 protein degradation *in vitro* and in the absence of chloroplast protein synthesis *in vivo*. *Photosynthesis Research* 41: 439–449.

van Aalst M, Ebenhöh O, Matuszyńska A. 2021. Constructing and analysing dynamic models with modelbase v1. 2.3: a software update. *BMC Bioinformatics* 22:1–15.

Watanabe CKA, Yamori W, Takahashi S, Terashima I, Noguchi K. 2016. Mitochondrial alternative pathway-associated photoprotection of photosystem II is related to the photorespiratory pathway. *Plant and Cell Physiology* 57:1426–1431.

Yamada S, Ozaki H, Noguchi K. 2020. The mitochondrial respiratory chain maintains the photosynthetic electron flow in *Arabidopsis thaliana* leaves under high-light stress. *Plant and Cell Physiology* 61:283–295.

Zaks J, Amarnath K, Kramer DM, Niyogi KK, Fleming GR. 2012. A kinetic model of rapidly reversible nonphotochemical quenching. *Proceedings of the National Academy of Sciences* 109:15757–15762.

Zavafer A. 2021. A theoretical framework of the hybrid mechanism of photosystem II photodamage. *Photosynthesis Research* 149: 107–120.